Evaluation of Thick Silicon Nitride Film Properties at 300 mm Scale for High-Q Photonic Devices

Soumen Kar, Senior Member, IEEE, Nicholas W. Gangi, Katrina A. Morgan, Lewis G. Carpenter, Nicholas M. Fahrenkopf, Yukta Timalsina, Christopher V. Baiocco, David Harame, Fellow, IEEE

Abstract—This work evaluates thick silicon nitride (SiN) film properties using various inline and offline advanced metrology data analysis. The thick SiN films for photonic applications are typically prepared by plasma-enhanced chemical vapor deposition (PECVD) and low-pressure chemical vapor deposition (LPCVD) techniques. Our present study combines high-volume inline and high-accuracy offline metrology to best characterize our thick SiN films. The developed SiN film compositional analysis has been carried out using inline X-ray photoelectron spectroscopy (XPS) to get fast feedback on the composition and contamination of the film surface. Finally, we present a refractive index (n) comparison for annealed and unannealed PECVD/LPCVD wafers.

Index Terms—Advanced metrology, annealed, composition, LPCVD, thick SiN, PECVD, refractive index, VASE, XPS.

I. INTRODUCTION

HICK silicon nitride (SiN) films have been demonstrated as an optical waveguide platform for passive and active photonic devices with low optical losses and a large transparency window spanning telecommunications and visible wavelengths [1], [2]. Much of the recent work in thick SiN (~>500 nm) is driven by Kerrcomb device development in which the dispersion requirements for a favorable nonlinear interaction drive the need for thick SiN. At 300 mm scale, the high film stress of

This material is based on research sponsored by the Air Force Research Laboratory under AIM Photonics (agreement number FA8650-21-2-1000). The U.S. Government is authorized to reproduce and distribute reprints for Governmental purposes notwithstanding any copyright notation thereon. The views and conclusions contained herein are those of the authors and should not be interpreted as necessarily representing the official policies or endorsements, either expressed or implied, of the United States Air Force, the Air Force Research Laboratory or the U.S. Government.

Soumen Kar, Lewis G. Carpenter, Yukta Timalsina, Christopher V. Baiocco and David Harame are with the American Institute for Manufacturing Integrated Photonics (AIM Photonics), Albany, NY 12203, USA (e-mail: skar@aimphotonics.com).

Nicholas W. Gangi was with the American Institute for Manufacturing Integrated Photonics (AIM Photonics), Albany, NY 12203, USA for his internship. He is now with the Rensselaer Polytechnic Institute (RPI), Troy, NY, USA 12180.

Katrina A. Morgan was with the American Institute for Manufacturing Integrated Photonics (AIM Photonics), Albany, NY 12203, USA. She is now with the University of Southampton, Southampton UK SO17 1BJ.

Nicholas M. Fahrenkopf was with the American Institute for Manufacturing Integrated Photonics (AIM Photonics), Albany, NY 12203, USA. He is now with the Northeast Regional Defense Technology Hub (NORDTECH), Albany, NY, USA 12203.

Color versions of one or more of the figures in this article are available online at http://ieeexplore.ieee.org

SiN prevents thick (>400 nm) films of high optical quality from being manufactured because significant and detrimental cracking occurs due to large wafer bow, severely limiting device yield with lower Q [3]. SiN films are commonly grown by plasma-enhanced chemical vapor deposition (PECVD) or low-pressure chemical vapor deposition (LPCVD). When PECVD is used, the films require annealing at temperatures above 1000°C to achieve low propagation losses by reducing the number of N-H bonds in the film and to out-diffuse the hydrogen [1], [4]. Specifically, N-H bonds act as absorption centers, and their low-energy tail leads to undesirable absorption loss in the region of 1510-1565 nm [5], [6], [7]. The major impurities in a-Si:H are O, C, and N, while those in SiN are H, O, C, F, Cl, and excess Si [8]. Impurities present in SiN can considerably impact its optical properties, including the refractive index, absorption coefficient, and bandgap, making the material's optical behavior highly dependent on the level and type of impurities incorporated during its synthesis or processing [9]. Therefore, a compositional analysis is required for the developed SiN film.

1

In this paper, we carried out inline wafer bow measurements, optical ellipsometry, and atomic force microscopy (AFM) on thick SiN films prepared by PECVD and LPCVD techniques. Inline ellipsometry provided thickness measurements on the SiN films and its refractive index at a 633 nm wavelength. To extract the film stoichiometry, we used an inline X-ray photoelectron spectroscopy (XPS) survey on the top surface of the thick SiN film to get rapid feedback on the composition and contamination of the film surface. Furthermore, we obtained the film thickness of PECVD- and LPCVD-grown samples using offline Scanning Electron Microscopy (SEM) and compared them with the inline measurement data. Additionally, a refractive index (n) comparison was obtained from offline variable angle spectroscopic ellipsometry (VASE) and verified with prism coupling to ensure index accuracy of the annealed and unannealed wafers. By combining both inline and offline metrology, we enable the verification and increased accuracy of refractive index measurements.

II. HIGH-Q WAVEGUIDE THICKNESS-WIDTH OPTIMIZATION

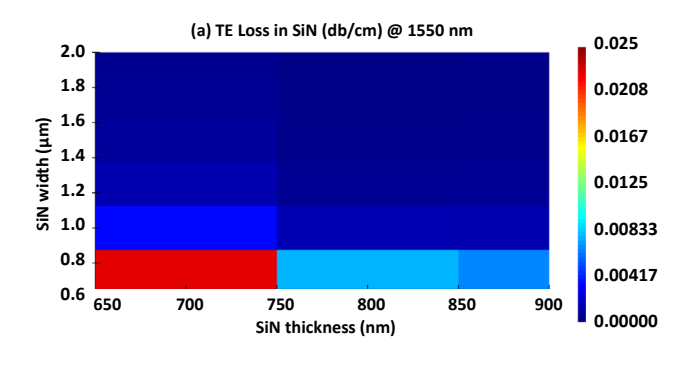
A. Numerical Model and Simulation

To achieve SiN waveguides with anomalous dispersion, we modeled different SiN waveguide widths and thicknesses using a 3- μ m BOX to find which dimensions yield anomalous dispersion. This is important for efficient Kerr nonlinear generation and the subsequent comb generation in SiN high-Q

© 2025 IEEE. All rights reserved, including rights for text and data mining and training of artificial intelligence and similar technologies. Personal use is permitted, but republication/redistribution requires IEEE permission. See https://www.ieee.org/publications/rights/index.html for more information.

ring resonators. To calculate propagation loss and dispersion for different SiN thicknesses and widths, a Finite Difference Eigenmode (FDE) solver was used [10], [11].

As shown in Fig. 1(a, b), our simulation shows the propagation loss and dispersion for the fundamental transverse electric (TE) mode at 1550 nm wavelength. Low propagation losses and anomalous dispersion are shown for >700-nm thick and >1.2- μ m wide SiN films.



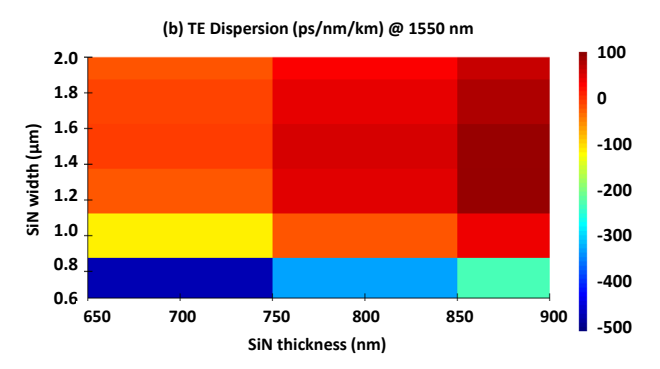


Fig. 1. Fundamental TE mode (a) propagation loss and (b) dispersion for varying SiN waveguide geometries at 1550 nm wavelength.

III. EXPERIMENTAL DETAILS

A. Sample Preparation

The blanket thick SiN films on 300 mm wafers were fabricated in experimental studies using PECVD and LPCVD processes. The PECVD process used low processing temperatures (<500°C) for the blanket SiN deposition of the front side of bare Si wafers and 3 µm buried oxide (BOX) wafers, leading to larger hydrogen impurities compared to higher temperature processes. However, LPCVD blanket SiN film is deposited on both sides of the bare Si wafer at a much higher process temperature (~800°C) and contains fewer hydrogen impurities. Some PECVD and LPCVD wafers are annealed at high temperatures (>1000°C) to reduce N-H and Si-H bonds. These impurities are responsible for a loss at telecommunication wavelengths, so it is important to remove them [11], [12]. After preparing these SiN wafers, we performed various inline and offline measurements to check the film thickness, roughness, stoichiometry, and composition. The following sub-sections will summarize the results.

B. Inline Measurements of the Wafers

As shown in Fig. 2, LPCVD SiN film did not show any significant wafer bow (or film stress) after SiN deposition, but PECVD SiN on bare Si showed very high compressive stress. Due to significant tensile stress, the PECVD SiN with BOX showed a negative wafer bow for SiN thicknesses >400-nm. Due to the larger bow, annealed PECVD wafers could not be measured. However, LPCVD annealed wafers showed very high compressive stress with a positive wafer bow for SiN films with thicknesses >200-nm. These results indicate that the bow induced by PECVD and high-temperature annealing respectively needs to be monitored closely through inline metrology in manufacturing to ensure high yield, while LPCVD has a higher tolerance due to lower stress [11].

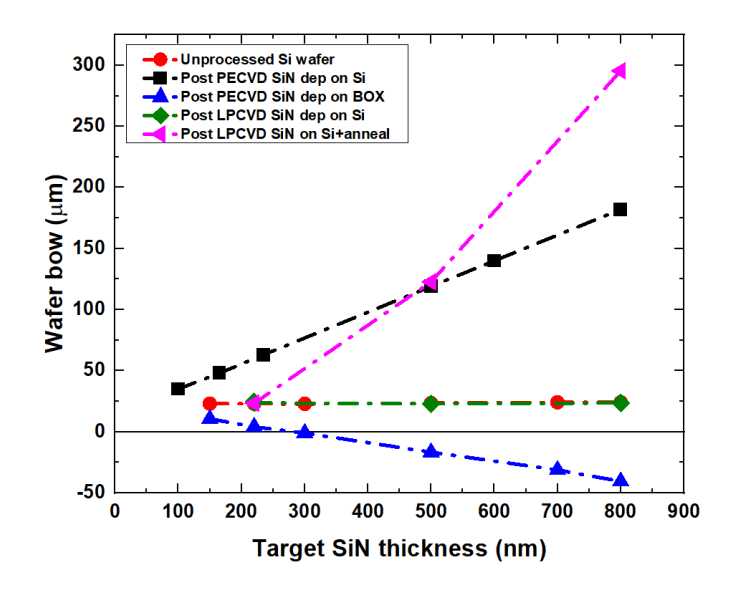
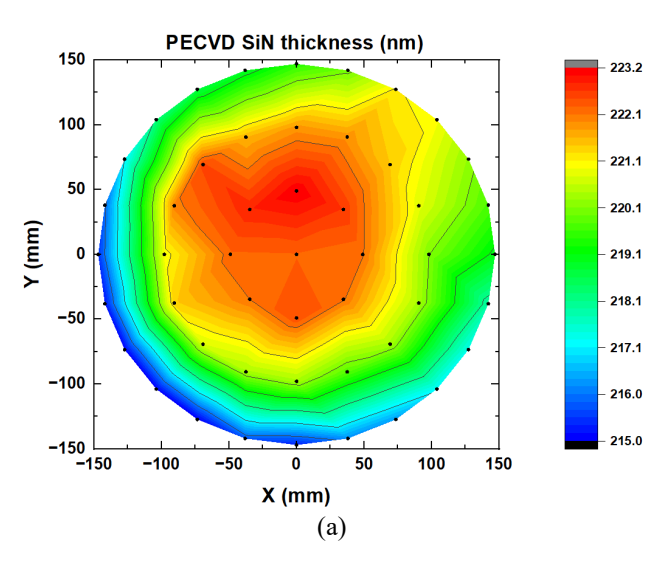


Fig. 2. SiN waveguide geometries at 1550 nm wavelength. Target SiN film thickness versus blanket wafer bow measured using inline KLA SpectraFilm LD10 tool demonstrating temperature dependency of stress.

The same inline KLA SpectraFilm LD10 tool is used to obtain a 49-point contour map for PECVD and LPCVD SiN film thickness (t) and refractive index at an optical wavelength of 633 nm. Fig. 3(a, b) shows the PECVD and LPCVD SiN film thickness, respectively. It is observed that the PECVD film is thicker at the center and thinner at the edge, with a thickness difference (Δt) of 8.2 nm. However, LPCVD film is the opposite, and it is thicker at the edge and thinner at the center with a thickness difference (Δt) of 4.5 nm. These results clearly show good center-to-edge thickness uniformity for both PECVD and LPCVD 300 mm wafers. At the same time, we obtained a refractive index (n) at an optical wavelength of 633 nm for PECVD and LPCVD unannealed and annealed wafers, as shown in Fig. (4-7), respectively. These inline refractive index data are further compared with offline VASE measurement data.

Fig. 4 and 5 show that the refractive index variation across the unannealed PECVD wafer is ≤0.45% and ≤0.34% for the annealed PECVD wafer. With annealing, the refractive index is increased by 2.0% for PECVD wafers. Fig. 6 and 7 show that the refractive index variation across the unannealed LPCVD wafer is ≤0.55% and ≤1.04% for the annealed LPCVD wafer. With annealing, the refractive index is increased by 1.0% for LPCVD wafers. Inline refractive index data in Figs. (4-7) shows that the unannealed LPCVD films had a higher refractive index than the PECVD wafers (Δn of 0.038-0.04 at 633 nm), and annealed films show similar nvalues for both PECVD and LPCVD films. The increase in refractive index upon annealing is in agreement with expectations of temperature dependency of refractive index. LPCVD films having a higher refractive index than PECVD also follow this temperature dependency trend with refractive index, as LPCVD has a higher processing temperature.



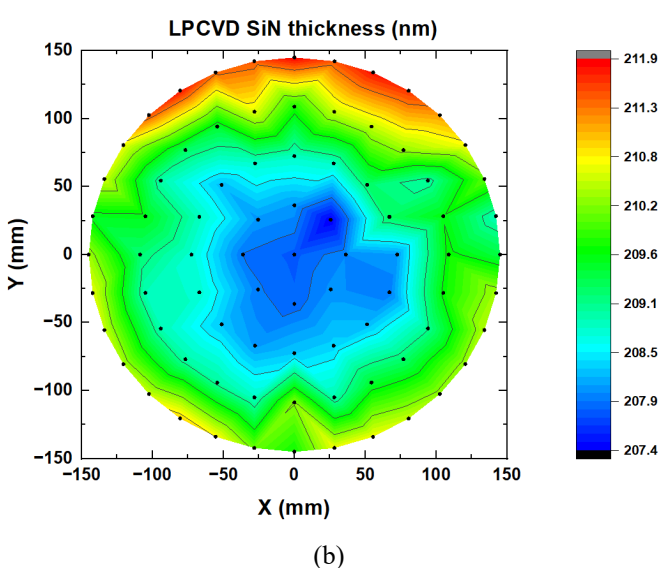


Fig. 3. (a) PECVD and (b) LPCVD SiN film thickness (t) measured using inline KLA SpectraFilm LD10 tool.

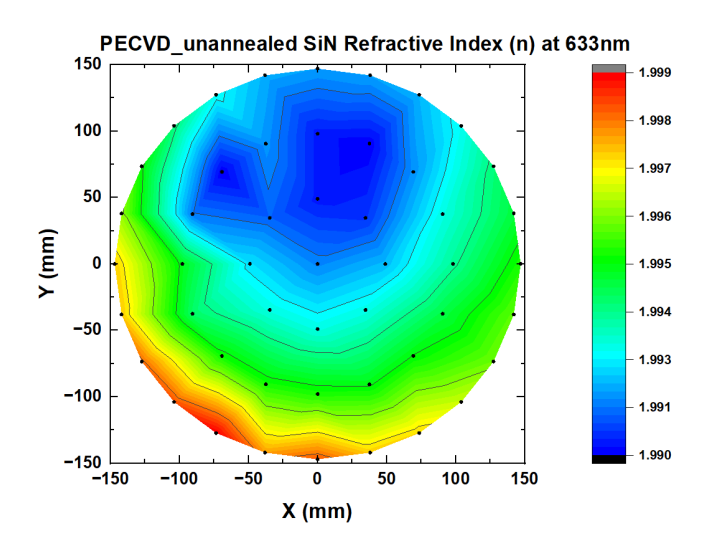


Fig. 4. Refractive index (*n*) at 633 nm of PECVD unannealed SiN wafer was measured using the inline KLA SpectraFilm LD10 tool.

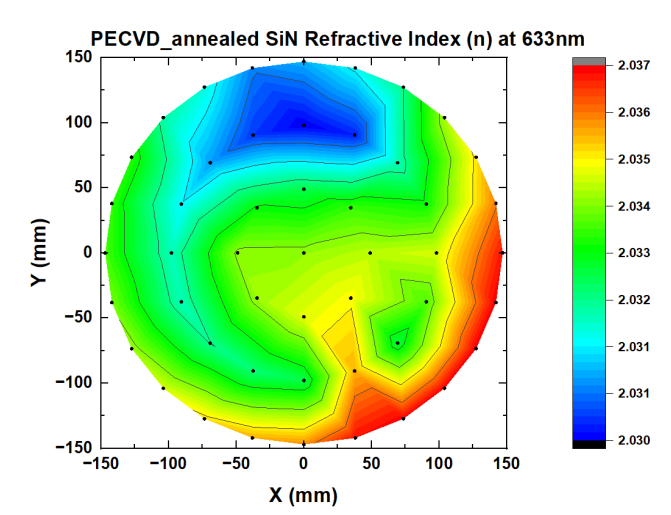


Fig. 5. Refractive index (*n*) at 633 nm of PECVD annealed SiN wafer measured using inline KLA SpectraFilm LD10 tool.

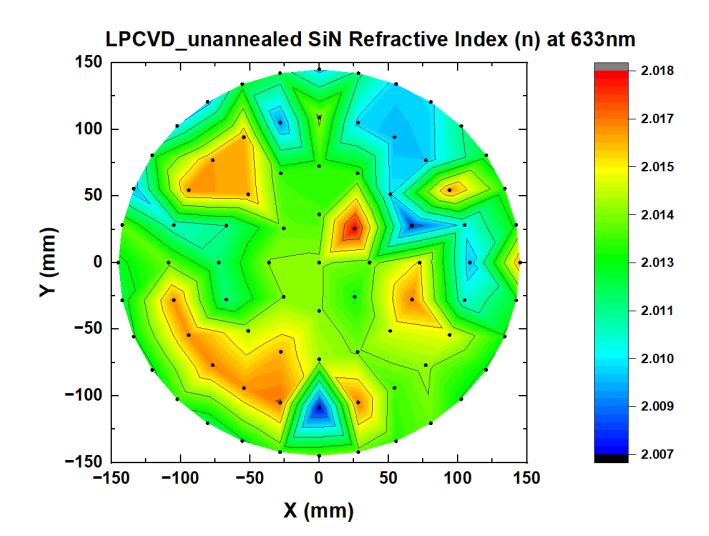


Fig. 6. Refractive index (n) at 633 nm of LPCVD unannealed SiN wafer measured using inline KLA SpectraFilm LD10 tool.

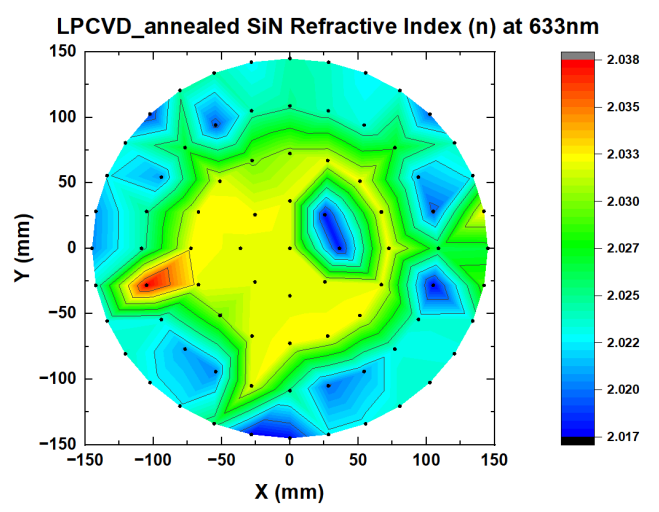
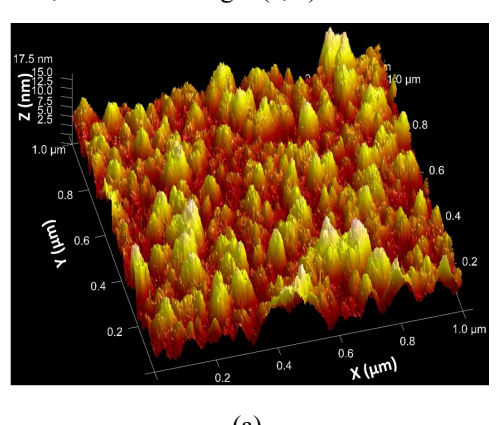


Fig. 7. Refractive index (n) at 633 nm of LPCVD annealed SiN wafer measured using inline KLA SpectraFilm LD10 tool.

The inline atomic force microscopy (AFM) study shows that the PECVD SiN films are 4-5 times rougher than the LPCVD films, as shown in Fig. 8(a, b).



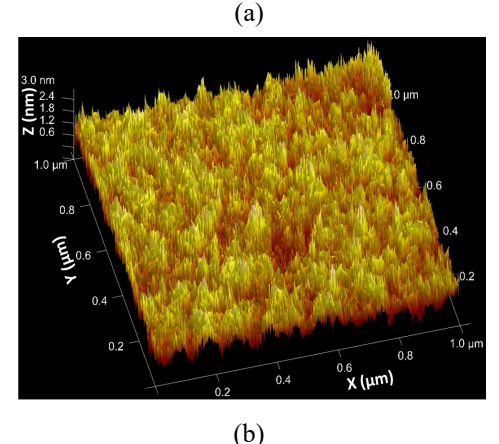


Fig. 8. 1×1μm² AFM surface area profile of 500 nm thick (a) PECVD (b) LPCVD films.

The AFM study is carried out in a 1.0-µm² area, and the PECVD wafer showed a 4.76-5.35% surface area difference, whereas the LPCVD wafer showed a 1.48-1.6% surface area difference. Fig. 9 shows RMS surface roughness from inline AFM as a function of film thickness and it displays a drastic increase in roughness while also exhibiting an increase in film

thickness for PECVD films. AFM roughness indicates LPCVD wafers are preferable for photonic device manufacturing as surface roughness leads to scattering [13], but chemical mechanical planarization (CMP) can be used to polish PECVD wafers for photonic applications.

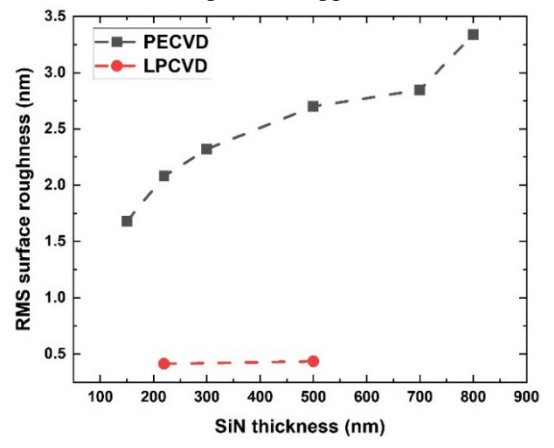


Fig. 9. RMS surface roughness from inline AFM as a function of film thickness.

For compositional analysis, the inline XPS was carried out in a Nova VeraFlex 3+ XPS system, using an Al K α (1486.6 eV) X-ray beam of 50 μ m in diameter. Low-resolution surveys were measured using a pass energy of 141.2 eV and an energy range from 0 eV to 1000 eV. The inline XPS provides fast feedback on composition and contamination.

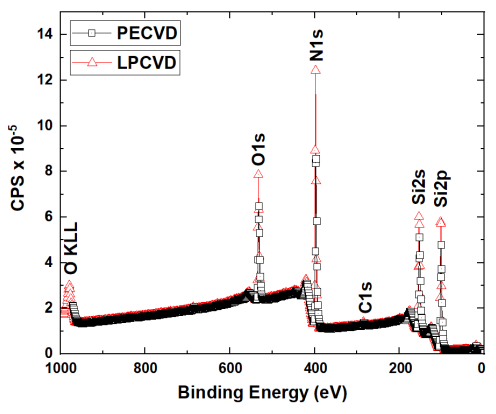


Fig. 10. Inline low-resolution XPS survey wide scan spectrum (0-1000 eV binding energy range), collected for PECVD and LPCVD SiN films.

Fig. 10 shows the low resolution inline XPS survey scan for the 0-1000 eV binding energy range collected for PECVD and LPCVD SiN films. The inline XPS provides fast feedback on composition and contamination. The survey spectrum shows the N1s, Si2s, and Si2p core XPS regions associated with Si3N4 and a C1s region associated with surface hydrocarbon from the PECVD and LPCVD processes. The O1s region comes from some SiO2 arising from the PECVD and LPCVD processes. The O KLL Auger features are also seen. These low-intensity X-ray satellite features (O KLL) can be seen to have higher binding energy of O1s peaks. Table I lists the binding energies associated with Si2p, Si2s, C1s, N1s, and O1s peaks and the reported literature values.

The Si2p spectra are characterized by doublet terms Si2p_{3/2} and Si2p_{1/2} due to spin-orbit coupling and are equal to 0.6 eV [14], [15]. Table I reports the Si2p_{3/2} binding energy and the main peak is observed at 101.6 eV for PECVD and 102.7 eV for LPCVD film. The Si2s peak is observed at 152.7 eV and 153.7 eV for PECVD and LPCVD films respectively. The N1s peak is observed at 397.4 eV for PECVD and 397.8 eV for LPCVD film. No substantial difference was observed in the O1s and C1s spectra, except for the variation in the integrated intensity of each spectrum. The dominant feature in the O1s spectra is a main peak at 531.2 eV for PECVD and 532.4 eV for LPCVD film, which can be considered to originate wholly from an O-Si environment of SiO₂ [16]; the principal peak in the C1s spectra is observed at 284.5 eV for PECVD and 284.6 eV for LPCVD films and identified as amorphous carbon, graphite and/or hydrocarbon on the top surface of the films.

 $TABLE\ I \\ BINDING\ ENERGIES\ OF\ XPS\ SURVEY\ SPECTRA\ FROM\ BEST\ FITTINGS$

Spectrum	Binding energies (eV)					
	PECVD LPCVD		Literature data			
Si2p _{3/2}	101.6±0.2	102.7±0.2	101.6 [17], 102.0 [18], 103.3 [19],			
			103.7 [20]			
Si2s	152.7±0.3	153.7±0.2	~151.0- 153.0 [21]			
C1s	284.5±0.2	284.6±0.1	284.4 [22], 284.38 [23], 285.0[23]			
N1s	397.4±0.3	397.8±0.2	397.1 [14], 397.4 [18]			
Ols	531.2±0.2	532.4±0.1	532.0 [16], 532.4 [22], 532.62[23]			

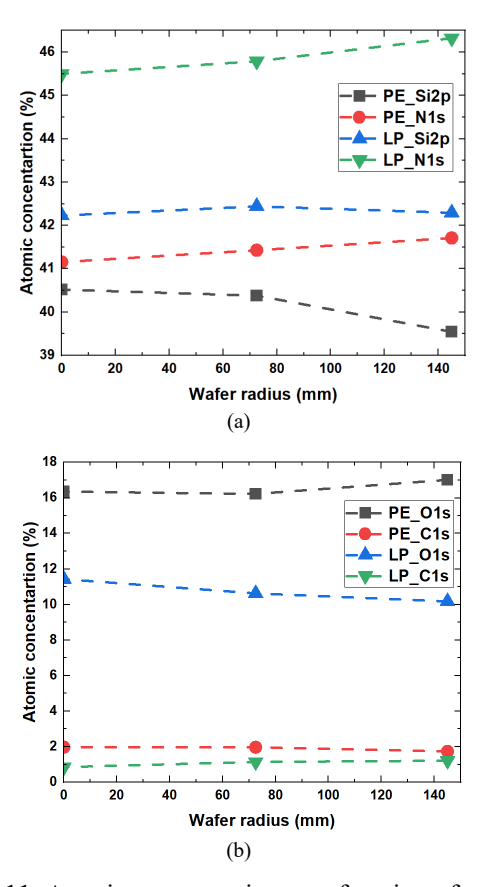


Fig. 11. Atomic concentration as a function of wafer radius for unannealed PECVD and LPCVD films XPS spectra with (a) Si2p and N1s peaks, (b) O1s and C1s peaks.

Fig. 11 (a, b) shows the atomic concentration as a function of wafer radius obtained from XPS survey spectrum Si2p, N1s, O1s and C1s peaks for unannealed PECVD and LPCVD films. This data gives useful information about the film composition at a 300 mm wafer scale and demonstrates excellent center-to-edge uniformity in film composition. PECVD films have more O1s and C1s content than LPCVD films. From the above results, we got N-deficient films in both PECVD and LPCVD, but PECVD has larger N deficiency when compared to LPCVD films.

C. Offline Measurements of the Wafers

Fig. 12 (a-c) showed the SEM cross-section of unannealed PECVD on bare Si and with BOX and unannealed LPCVD on Si samples with 820-, 824-, and 790-nm thick SiN, respectively. The measured cross-section thickness is within $\pm 3\%$ of its target thickness and verifies the reliance on inline thickness measurements [11].

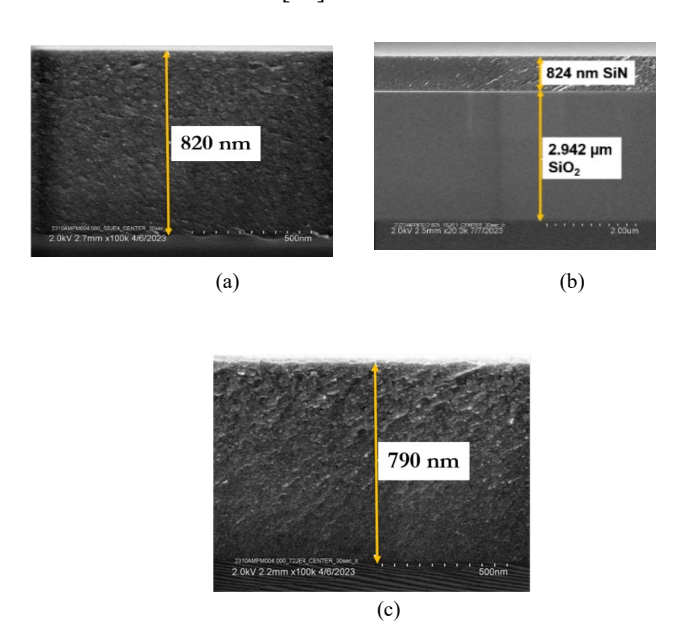


Fig. 12. SEM cross-section of unannealed (a) PECVD SiN on bare Si, (b) PECVD SiN on BOX (to demonstrate successful growth on different substrates, required for device manufacturing where growth on BOX and Si wafers is standard), and (c) LPCVD SiN on bare Si wafers.

Fig. 13 (a-c) compares measured xSEM thickness with a thickness measured using inline KLA SpectraFilm LD10 tool as a function of wafer radius for 220 nm, 500 nm, 800 nm PECVD and LPCVD SiN films. It is observed that the PECVD film is thicker at the edge of the wafer than in its center. However, LPCVD films are thinner at the center than the edge. The xSEM thickness variation is within the $\sim\pm2\%$ to $\pm4\%$ range compared to the inline KLA SpectraFilm LD10 measurements. The refractive index of PECVD and LPCVD wafers was obtained using an offline M-2000 J. A. Woollam Variable Angle Spectroscopic Ellipsometer (VASE) and a prism coupling method (Metricon Model 2010/M).

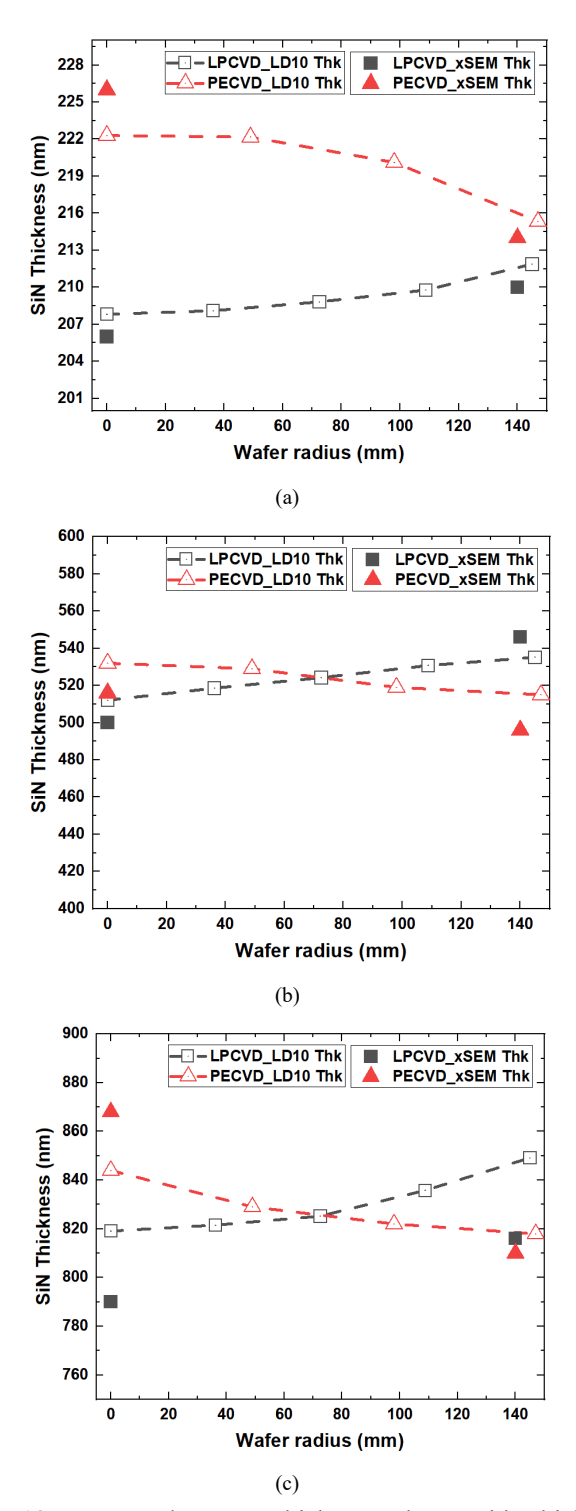


Fig. 13. Measured xSEM thickness along with thickness measured using inline KLA SpectraFilm LD10 tool as a function of wafer radius for PECVD and LPCVD (a) 220 nm, (b) 500 nm and (c) 800 nm SiN films.

Fig. 14(a) shows that the unannealed LPCVD films had a higher refractive index than unannealed PECVD wafers (Δn of 0.017 at 633 nm and 0.021 at 1550 nm). This is consistent with expectations due to higher processing temperatures. LPCVD film data is consistent with the refractive index

provided in reference [10]. Using a prism coupling method (Metricon Model 2010/M), the refractive index was measured at 637 nm (n = 2.025), 853 nm (n = 2.0112) and extrapolated to 1550 nm (n = 1.9934). These refractive index values were then used as references to increase the accuracy of the ellipsometry fitting models [11].

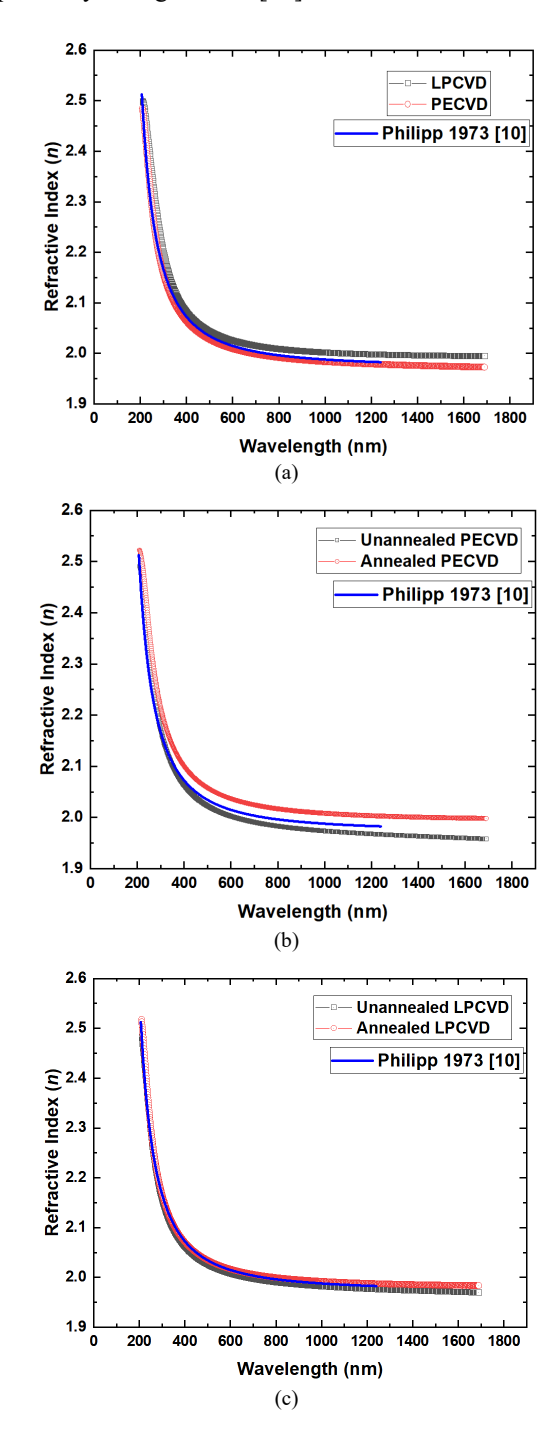


Fig. 14. Refractive index versus wavelength (a) compared for PECVD and LPCVD deposition techniques, (b) for PECVD annealed and unannealed wafers, (c) for LPCVD annealed and unannealed wafers along with the refractive index provided in reference [10].

TABLE II
REFRACTIVE INDEX IN VISIBLE AND TELECOMMUNICATION WAVELENGTHS

Wavelength (nm)	Refractive index (n)				
()	PECVD unannealed	PECVD annealed	LPCVD unannealed	LPCVD annealed	
633 (inline)	1.9940	2.0336	2.0091	2.0156	
633 (offline)	1.9983	2.0321	2.0049	2.0112	
1550 (offline)	1.9611	1.9991	1.9744	1.9828	

Table II shows the refractive index obtained from the inline optical ellipsometry and the combined offline VASE and prism coupling measurements of SiN in visible and telecommunication wavelengths. The reported refractive index values in Table II agree with the literature values [10], [11].

Fig. 14(b, c) shows annealing versus refractive index (n) at various wavelengths for PECVD and LPCVD wafers, respectively. As shown in Table II and Fig. 11(a-c), process temperature and annealing have a more significant effect on the refractive index of PECVD films than LPCVD films, which can be explained by the larger increase in the thermal budget of ~500°C, compared to 200°C. As we compare these offline VASE data with our previously obtained inline refractive index data at 633 nm (Table II), we found that both data corroborate. The inline data gave us the refractive index at 633 nm and the thickness map for the whole wafer. However, offline data gave us the refractive index at a wide range of wavelengths to determine the suitability of the SiN film at the 300-mm scale for device fabrication [11].

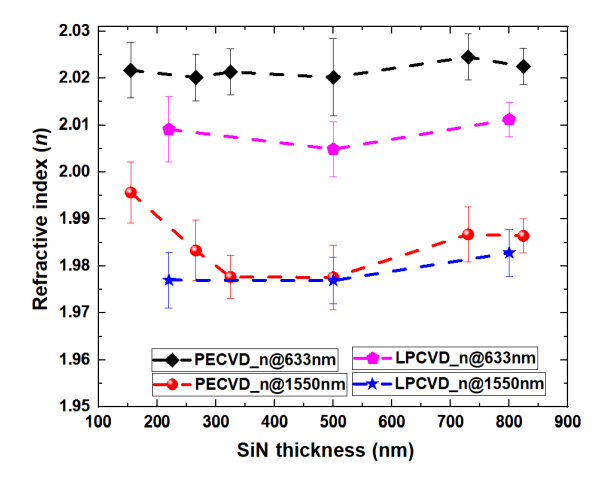


Fig. 15. Annealed PECVD and annealed LPCVD SiN refractive index versus thickness at 633 nm and 1550 nm wavelength.

In Fig. 15, the refractive index at 633 nm and 1550 nm wavelengths as a function of annealed PECVD and LPCVD SiN thickness is shown. This measurement was performed at the center and edge of the wafers for both PECVD and LPCVD films. We did not observe any significant difference in the refractive index obtained from VASE for the center and edge of the wafers. It is also observed that the SiN refractive

index had no significant dependency on increasing film thickness.

IV. CONCLUSION

In this paper, we performed various inline and offline measurements for thick, unannealed and annealed PECVD and LPCVD SiN films. We compared inline and offline thickness data, and the variation is within a $\sim \pm 2\%$ to $\pm 4\%$ range. We also obtained excellent center-to-edge thickness uniformity at a 300 mm scale. The inline XPS survey spectrum shows the N1s, Si2s, and Si2p core XPS regions associated with stoichiometric Si₃N₄ along with a C1s region associated with surface hydrocarbon from the PECVD and LPCVD processes. The O1s region comes from some SiO₂ arising from the PECVD and LPCVD processes. The atomic concentration as a function of wafer radius is obtained from XPS survey spectrum Si2p, N1s, O1s and C1s peaks for unannealed PECVD and LPCVD films. This data gives ≤5% variation in the film composition at a 300 mm wafer scale and demonstrates excellent center-to-edge uniformity in film composition. The inline ellipsometry data showed annealed PECVD films with a mean refractive index (633 nm) of 2.0336 for 150-825 nm thick films. Similarly, annealed LPCVD films are shown to have a mean refractive index (633 nm) of 2.0156 for 220-800 nm thick films. These data are in good agreement with offline VASE data. This refractive index characterization provides vital input for accurate photonic device design, defining surface quality through AFM roughness measurement for thick film/device and bow measurement to ensure manufacturing tolerance is met. Our recent SiN blanket film results underscore the potential to develop SiN-based active and passive devices for nextgeneration high-Q photonic applications using 300 mm wafers.

ACKNOWLEDGMENT

The authors gratefully acknowledge the support of the Engineers and Technicians of AIM Photonics, Albany, NY for this work. We also acknowledge the support of the Metrology and Failure Analysis (FA) teams of the New York Center for Research, Economic Advancement, Technology, Engineering and Science (NY CREATES) in Albany, NY, for all metrology experiments and SEM cross-section images.

REFERENCES

- [1] S. C. Mao et al., "Low propagation loss SiN optical waveguide prepared by optimal low-hydrogen module," *Opt. Express*, vol. 16, pp. 20809-20816, 2008, doi: 10.1364/OE.16.020809. https://doi.org/10.1364/OE.16.020809
- [2] C. R. Doerr et al., "Potentially low-cost widely tunable laser consisting of a semiconductor optical amplifier connected directly to a silica waveguide grating router," *IEEE Photon. Technol. Lett.* vol. 15, pp. 1446-1448, 2003, doi: 10.1109/LPT.2003.818244.
- [3] K. Luke, A. Dutt, C. B. Poitras, and M. Lipson, "Overcoming Si₃N₄ film stress limitations for high quality factor ring resonators," *Opt. Express*, vol. 21, pp. 22829-22833, 2013, doi: 10.1364/OE.21.022829.
- [4] J. M. Olson, "Analysis of LPCVD Process Conditions for the Deposition of low stress silicon nitride. Part I: Preliminary LPCVD experiments," *Mater. Sci. Semicond. Process*, vol.5, pp. 51-60, 2002. https://doi.org/10.1016/S1369-8001(02)00058-6

- [5] F. Ay, A. Aydinli, "Comparative investigation of hydrogen bonding in silicon based PECVD grown dielectrics for optical waveguides," Opt. Mater., vol. 26, pp. 33-46, 2004. https://doi.org/10.1016/j.optmat.2003.12.004
- [6] F. L. Martinez, R. Ruiz-Merino, A. del Prado, E. San Andres, I. Martil, G. Gonzalez-Diaz, G. Jeynes, N. P. Barradas, L. Wang, H. S. Reehal, "Bonding structure and hydrogen content in silicon nitride thin films deposited by electron cyclotron resonance plasma method," *Thin Solid Films*, vol. 459, pp. 203-207, 2004. https://doi.org/10.1016/j.tsf.2003.12.084
- [7] D. K. T. Ng et al., "Exploring high refractive index silicon-rich nitride films by low-temperature inductively coupled plasma chemical vapor deposition and applications for integrated waveguides", ACS Appl. Mater. Interfaces, vol. 7, pp. 21884–21889, 2015. https://doi.org/10.1021/acsami.5b06329
- [8] C.C. Tsai, M.J. Thompson & H.C. Tuan, "Impurities in Bulk A-Si:H, Silicon Nitride, and at the a-Si:H/Silicon Nitride Interface". MRS Online Proceedings Library, vol. 33, pp. 297–300, 1984. https://doi.org/10.1557/PROC-33-297
- [9] E. Kutlu, et al., "Effect of substitutional As impurity on electrical and optical properties of β-Si3N4 structure", *Materials Research Bulletin*, vol. 83, pp. 128-134, 2016. https://doi.org/10.1016/j.materresbull.2016.05.017
- [10] H. R. Philipp, "Optical Properties of Silicon Nitride," Jr. Electrochem. Soc., vol. 120, no. 2, p. 295, 1973, doi: 10.1149/1.2403440. doi: 10.1149/1.2403440
- [11] S. Kar, N. W. Gangi, K. A. Morgan, L. G. Carpenter, N. M. Fahrenkopf and C. V. Baiocco, "Advanced Metrology of Thick Silicon Nitride Films at 300 mm Scale for Next Generation High-Q Photonic Devices," 2024 35th Advanced semiconductor manufacturing conference (ASMC), Albany, NY, USA, 2024, pp. 1-6, doi: 10.1109/ASMC61125.2024.10545523.
- [12] X. X. Chia et al., "Deuterated SiNx: a low-loss, back-end CMOS-compatible platform for nonlinear integrated optics," *Nanophotonics*, vol. 12, no. 8, pp. 1613–1631, Apr. 2023, doi: 10.1515/nanoph-2022-0626.1.
- [13] Sven Schröder, Angela Duparré, Luisa Coriand, Andreas Tünnermann, Dayana H. Penalver, and James E. Harvey, "Modeling of light scattering in different regimes of surface roughness," *Opt. Express*, vol. 19, pp. 9820-9835, 2011, doi: 10.1364/OE.19.009820.
- [14] M. Matsuoka, S. Isotani, W. Sucasaire, L.S. Zambom, K. Ogata, "Chemical bonding and composition of silicon nitride films prepared by inductively coupled plasma chemical vapor deposition", *Surf. & Coat. Technol.*, vol. 204, pp. 2923–2927, 2010. https://doi.org/10.1016/j.surfcoat.2010.02.071
- [15] C.D. Wagner, A.V. Naumkin, A. Kraut-Vass, J.W. Allison, C.J. Powell, J.R.Jr. Rumble, NIST Standard Reference Database 20, Version 3.4 (web version) (http://srdata.nist.gov/xps/) 2003.
- [16] H.-f. Li, S. Dimitrijev, D. Sweatman, H.B. Harrison, P. Tanner, "Investigation of nitric oxide and Ar annealed SiO₂/SiC interfaces by x-ray photoelectron spectroscopy", *J. Appl. Phys.*, vol. 86, pp. 4316-4321, 1999. https://doi.org/10.1063/1.371363
- [17] J. Viard, E. Beche, D. Perarnau, R. Berjoan, J. Durand, "XPS and FTIR study of silicon oxynitride thin films", *Jr. of the Euro. Ceram. Soc.*, vol. 17, Issues 15–16, pp. 2025-2028. 1997. https://doi.org/10.1016/S0955-2219(97)00051-4
- [18] I. Bertóti, "Characterization of nitride coatings by XPS", Surf. Coat. Technol., vol. 151–152, pp. 194 203, 2002. https://doi.org/10.1016/S0257-8972(01)01619-X
- [19] C.D. Wagner, D.E. Passoja, H.F. Hillery, T.G. Kinisky, H.A. Six, W.T. Jansen, J.A. J. Taylor, "Auger and photoelectron line energy relationships in aluminum—oxygen and silicon—oxygen compounds", *Vac. Sci. Technol.*, vol. 21, pp. 933- 944, 1982. https://doi.org/10.1116/1.571870
- [20] A.R. Gonzalez-Elipe, J.P. Espinos, G. Munuera, J. Sanz, J.M. J. Serratosa, "Bonding-state characterization of constituent elements in phyllosilicate minerals by xps and nmr," *Phys. Chem.*, vol. 92, pp. 3471-3476, 1988. https://doi.org/10.1021/j100323a031
- [21] Sekhar C. Ray, D. K. Mishra, A. M. Strydom, and P. Papakonstantinou, "Magnetic behavioural change of silane exposed graphene nanoflakes", *Jr. of Appl. Phys.*, vol. 118, P. 115302, 2015. doi: 10.1063/1.4930932

- [22] S. I. Zida, Y.D. Lin, Y. L. Khung, "Sonochemical Reaction of Bifunctional Molecules on Silicon (111) Hydride Surface", *Molecules*, vol. 26, P. 6166, 2021. https://doi.org/10.3390/molecules26206166
- [23] G. Beamson, D. Briggs, High Resolution XPS of Organic Polymers -The Scienta ESCA300 Database Wiley Interscience, pp. 268-269, 1992. https://doi.org/10.1021/ed070pA25.5